CHINESE OPTICS LETTERS

Vol. 19, No. 10 | October 2021

Perfect light absorption in monolayer MoS_2 empowered by optical Tamm states

Yangwu Li (李扬武), Hua Lu (陆 华)*, Jiadeng Zheng (郑佳灯), Shichang Li (李世昌), Xiao Xuan (宣 霄), and Jianlin Zhao (赵建林)**

MOE Key Laboratory of Material Physics and Chemistry under Extraordinary Conditions, Key Laboratory of Light-Field Manipulation and Information Acquisition, Ministry of Industry and Information Technology, and Shaanxi Key Laboratory of Optical Information Technology, School of Physical Science and Technology, Northwestern Polytechnical University, Xi'an 710129, China

*Corresponding author: hualu@nwpu.edu.cn

**Corresponding author: jlzhao@nwpu.edu.cn

Received January 16, 2021 | Accepted March 26, 2021 | Posted Online August 18, 2021

We present the perfect light absorption of monolayer molybdenum disulfide (MoS_2) in a dielectric multilayer system with two different Bragg mirrors. The results show that the strong absorption of visible light in monolayer MoS_2 is attributed to the formation of optical Tamm states (OTSs) between two Bragg mirrors. The MoS_2 absorption spectrum is dependent on the layer thickness of Bragg mirrors, incident angle of light, and the period numbers of Bragg mirrors. Especially, the nearly perfect light absorption (99.4%) of monolayer MoS_2 can be achieved by choosing proper period numbers, which is well analyzed by the temporal coupled-mode theory.

Keywords: optical Tamm states; molybdenum disulfide; light absorption.

DOI: 10.3788/COL202119.103801

1. Introduction

Atomically thinned materials including graphene, transition metal dichalcogenides (TMDCs), hexagonal boron nitride (hBN), MXenes, etc., exhibit fascinating electric, optical, mechanical, and thermal properties and attract broad interests in the fields of electronics, optoelectronics, and photonics[1–5]. In contrast to graphene, TMDCs are semiconductors with a direct bandgap, as they are exfoliated into monolayers, which advance the development of two-dimensional (2D) material photonics and optoelectronics[6]. As a typical TMDC, molybdenum disulfide (MoS_2) possesses a direct bandgap of 1.8 eV when reducing from bulk to monolayer[7]. In the MoS_2 monolayer, a hexagonal layer of Mo atoms is sandwiched between two hexagonal layers of S atoms in a trigonal prismatic arrangement. The atomic thickness and electronic band structure make MoS_2 an excellent candidate for achieving field effect transistors with an ultra-high on/off ratio[8]. Recently, MoS_2 has achieved numerous applications in photodetection[9,10], photoluminescence[11], mode-locking lasers[12,13], solar cells[14], and photovoltaic devices[15]. Nevertheless, the average single-pass light absorption of monolayer MoS_2 is approximately 10% in the visible wavelength range[16]. The intrinsically weak interaction between light and MoS_2 seriously hinders light harvesting and photoelectric conversion. Enhancing the light absorption of MoS_2 is of vital importance for realizing high-performance photoelectronic devices. Fortunately, some photonic structures have been reported to improve light absorption of monolayer MoS_2. A photonic crystal on a metallic mirror enabled an average light absorption of about 51% in monolayer MoS_2[16]. Wang *et al.* employed a Fano-resonant photonic crystal structure to increase the MoS_2 absorption up to 90%[17]. Bahauddin *et al.* designed a plasmonic architecture with silver nanoparticles to realize broadband MoS_2 absorption of 37%[18]. Luo *et al.* demonstrated an enhanced dual-band MoS_2 absorption of 57% and 87.5% by employing a metallic metamaterial with periodic nanoribbons and a flat substrate[19]. Based on an Al_2O_3/Al nanocavity, Janisch *et al.* boosted the light absorption of monolayer MoS_2 up to 70% utilizing the strong interference effect[20]. Enhancing light absorption has also been investigated in other atomic-layer materials, such as graphene, WSe_2, black phosphorus, etc.[21–24]. However, the light absorption efficiencies of the atomic-layer materials are limited in these photonic structures with the excitation of plasmonic or cavity-supported resonances. Optical Tamm states (OTSs) are a kind of highly confined interface modes formed at the interface between two different dielectric Bragg mirrors. The operating wavelength of OTSs exists in the overlapped photonic band gaps of two Bragg mirrors[25]. The lossless OTS mode can be directly excited in arbitrary polarizations and is independent of the incident angle, providing great potential for reinforcing the MoS_2 interaction with light and device capabilities[25,26].

In this Letter, we firstly propose to realize perfect light absorption of MoS_2 in a multilayer structure, consisting of a monolayer MoS_2 embedded between two different Bragg mirrors. Due to the excitation of OTS, the interaction between light and monolayer MoS_2 can be greatly enhanced, and thus the light absorption of MoS_2 can approach 99.4% in the visible range. Both the theoretical and simulation calculations illustrate that the light absorption of MoS_2 can be tailored by altering the layer thickness of Bragg mirrors, angle of incident light, and period number of Bragg mirrors. The temporal coupled-mode theory (TCMT) is employed to effectively analyze the light absorption evolution of MoS_2 with the period numbers of Bragg mirrors. Our results will offer a new way to enhance the interaction between light and atomic-layer materials and realize high-performance 2D material-based optoelectrical devices.

2. Structure and Model

Figure 1 shows the proposed multilayer photonic structure with a monolayer MoS_2 sandwiched in two all-dielectric Bragg mirrors. The Bragg mirrors are composed of the alternatively stacked silicon nitride (Si_3N_4) and silica (SiO_2) layers, whose refractive indices are set as $n_a = 2.05$ and $n_b = 1.46$, respectively[27,28]. The Si_3N_4 and SiO_2 layers can be deposited in turn by plasma-enhanced chemical vapor deposition[29]. The deposition rate and time can be controlled for the different layer thickness. Monolayer MoS_2 can be synthesized on a sapphire substrate with a large area by chemical vapor deposition and transferred by the wetting transfer method[14]. The thicknesses of the Si_3N_4 and SiO_2 layers are denoted by a_l and b_l (a_r and b_r) for the left (right) Bragg mirror, respectively. The period numbers of Bragg mirrors are P_l and P_r. The relative permittivity of monolayer MoS_2 can be determined by the Lorentz model[30,31]:

$$\varepsilon_r = \varepsilon_\infty + \sum_{k=1}^{K} \frac{a_k}{\omega_k^2 - \omega^2 - j\omega b_k}, \tag{1}$$

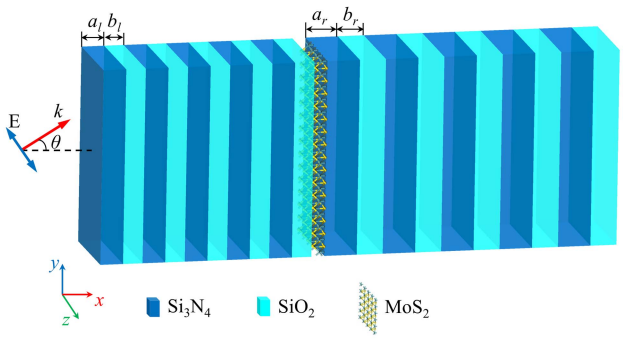

Fig. 1. Schematic diagram of the multilayer structure consisting of two different Bragg mirrors and a monolayer MoS_2 sandwiched in the Bragg mirrors. The thicknesses of Si_3N_4 and SiO_2 layers are denoted by a_l and b_l (a_r and b_r) for the left (right) Bragg mirror, respectively. The period numbers of the left and right Bragg mirrors are P_l and P_r, respectively. The light is incident from the left side of the structure.

where ε_∞, a_k, b_k, ω, and ω_k stand for the DC permittivity, oscillation power, damping factor of the kth oscillator, angular frequency of incident light, and resonance frequency of the kth oscillator, respectively. These parameters in the Lorentz model can be found in Ref. [31]. The thickness of the MoS_2 layer can be set as $h = 0.615$ nm[30,31]. With this value, the MoS_2 light absorption matched well with the experimental data[30,31].

The spectral response of multilayer structures can be theoretically calculated by the transfer matrix method (TMM)[32–34]. Our multilayer structure can be simplified as a combination of $2(P_l + P_r) + 1$ dielectric layers with $2(P_l + P_r) + 2$ interfaces. When a TM-polarized incident light impinges on the left side of the structure with an incident angle θ, the reflection and transmission coefficients of the ith interface are expressed as $r_i = (n_i \cos\theta_{i-1} - n_{i-1}\cos\theta_i)/(n_i \cos\theta_{i-1} + n_{i-1}\cos\theta_i)$ and $t_i = 2n_{i-1}\cos\theta_{i-1}/(n_i\cos\theta_{i-1} + n_{i-1}\cos\theta_i)$, respectively. n_i and θ_i stand for the refractive index and light propagation angle in the ith layer $[i = 1, 2, \ldots, 2(P_l + P_r) + 1]$, respectively. The relation between the propagation angles can be governed by Snell's law: $n_{i-1}\sin\theta_{i-1} = n_i \sin\theta_i$ ($\theta_0 = \theta$).

Based on Maxwell's equations and the continuity of tangential components for electric and magnetic field vectors at the boundaries, the transfer matrices $\mathbf{M}_i$ and $\mathbf{P}_i$ can be derived to characterize the evolution of electric field amplitudes when light passes through the ith interface and layer. They satisfy the relation as follows:

$$\begin{bmatrix} E_{i-1}^+ \\ E_{i-1}^- \end{bmatrix} = \begin{bmatrix} 1/t_i & r_i/t_i \\ r_i/t_i & 1/t_i \end{bmatrix} \begin{bmatrix} e^{-j\phi_i} & 0 \\ 0 & e^{j\phi_i} \end{bmatrix} \begin{bmatrix} E_i^+ \\ E_i^- \end{bmatrix} = \mathbf{M}_i\mathbf{P}_i \begin{bmatrix} E_i^+ \\ E_i^- \end{bmatrix}, \tag{2}$$

where E_{i-1}^+ and E_{i-1}^- represent the electric field amplitudes of incident and reflected light on the left side of the ith interface, respectively. ϕ_i is the phase shift for the light propagating over distance d_i in the ith layer, which can be expressed as $\phi_i = 2\pi d_i n_i \cos\theta_i/\lambda$. The overall transfer matrix $\mathbf{Q}$ of the multilayer structure can be obtained by multiplying all matrices in sequence,

$$\mathbf{Q} = \left[\prod_{i=1}^{2(P_r+P_l)+1} \mathbf{M}_i\mathbf{P}_i\right]\mathbf{M}_{2(P_r+P_l)+2} = \begin{bmatrix} Q_{11} & Q_{12} \\ Q_{21} & Q_{22} \end{bmatrix}. \tag{3}$$

The reflection, transmission, and absorption spectra of the multilayer structure can be calculated by $R = |Q_{21}/Q_{11}|^2$, $T = |1/Q_{11}|^2$, and $A = 1 - R - T$, respectively. By using the above TMM, we investigate the light propagation characteristics of the multilayer structure with only two dielectric Bragg mirrors (i.e., $h = 0$ nm). The dielectric layer thicknesses of Bragg mirrors are set as $a_l = 89$ nm, $b_l = 44$ nm, $a_r = 148$ nm, and $b_r = 130$ nm. Thus, the bandgaps of two Bragg mirrors can be overlapped, providing an essential condition for the excitation of OTSs[25]. The period numbers of the left and right Bragg mirrors are chosen as $P_l = 8$ and $P_r = 20$, respectively. As shown in Fig. 2(a), there is an obvious and narrow dip at the wavelength of 509.5 nm in the reflection spectrum. To verify the theoretical results, we use the finite-difference time-domain (FDTD) method to numerically simulate the light propagation in

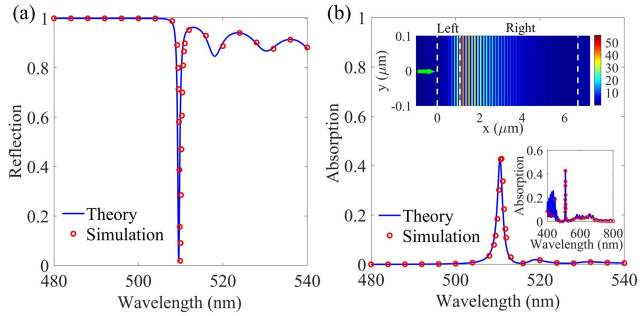

Fig. 2. (a) Reflection spectra in the multilayer structure with $P_l = 8$, $P_r = 20$, $a_l = 89$ nm, $b_l = 44$ nm, $a_r = 148$ nm, $b_r = 130$ nm, and $\theta = 0°$. (b) Light absorption spectra of the multilayer structure with a MoS_2 monolayer. The lines and circles represent theoretical and simulation results, respectively. The upper inset shows the field distribution of $|E|^2$ at the wavelength of 509.5 nm in the multilayer structure ($h = 0$ nm). The lower inset shows the spectrum of MoS_2 light absorption in the full visible range.

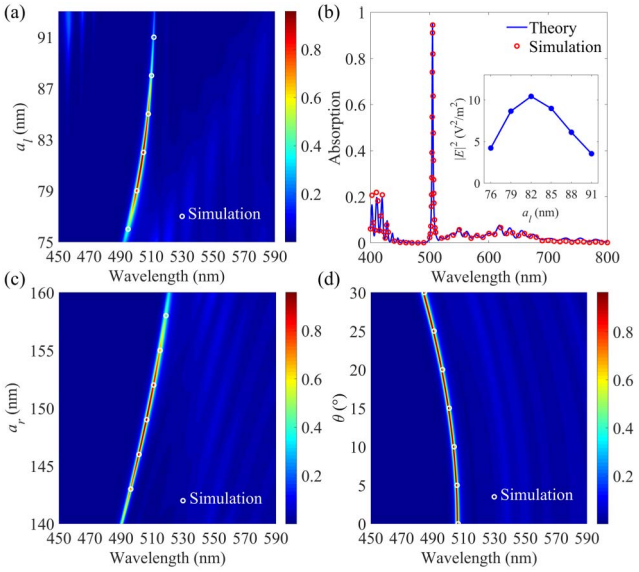

Fig. 3. (a) Evolution of MoS_2 light absorption spectrum with the Si_3N_4 layer thickness a_l in the structure with $a_r = 148$ nm and $\theta = 0°$. (b) Corresponding absorption spectrum of MoS_2 monolayer when $a_l = 82$ nm and $\theta = 0°$. The inset shows the dependence of electric field intensity in MoS_2 on a_l. (c) Evolution of MoS_2 light absorption spectrum with the thickness a_r when $a_l = 82$ nm and $\theta = 0°$. (d) Evolution of MoS_2 light absorption spectrum with θ when $a_l = 82$ nm and $a_r = 149$ nm. The circles denote the simulation results. Here, $P_l = 8$, $P_r = 20$, $b_l = 44$ nm, and $b_r = 130$ nm.

multilayer structures (Lumerical FDTD Solutions)[35]. For the convergence of simulations, the custom non-uniform mesh is adopted, and the maximum mesh steps along the x and y directions are set as $\Delta x = 1$ nm and $\Delta y = 5$ nm. The simulation time is set as 8000 fs with an auto shutoff level of 10^{-10}. The mesh size of MoS_2 layer is 0.1 nm. The electric field amplitude of incident light is set as 1 V/m. The simulation results agree well with the TMM results, as shown in Fig. 2(a). According to the TMM calculated reflection spectra of two separate Bragg mirrors, the dip wavelength (509.5 nm) is exactly located in the overlapped region of the two photonic bandgaps (not shown here). To prove the formation of OTS, the field intensity distribution of $|E|^2$ at the dip wavelength is simulated via the FDTD method, as depicted in the upper inset of Fig. 2(b). The white dotted boxes show the areas of two Bragg mirrors. We can see that the electric field is mostly confined around the interface, and the intensity is enhanced by over 50 folds. Both the reflection dip in the overlapped bandgap and strongly confined electric field indicate the existence of OTS at the interface between two Bragg mirrors. It can contribute to the strong boosting of light–matter interaction[25]. To explore OTS-assisted light–matter interaction, we introduce a monolayer MoS_2 sandwiched between the two Bragg mirrors, as shown in Fig. 1. Figure 2(b) shows the absorption spectra of the multilayer structure with the MoS_2 monolayer. We can see that the absorption spectrum of MoS_2 exhibits a distinct peak with a height of 43.0% at the wavelength of 510.5 nm. The theoretical calculations agree well with the numerical simulations. Because of the OTS excitation, the electric field intensity in the MoS_2 monolayer at the absorption peak wavelength is enhanced to 5.2 V^2/m^2. Thus, the reinforced light absorption can be attributed to the OTS field confined at the interface of Bragg mirrors.

3. Results and Analysis

Subsequently, we investigate the relation between the Bragg layer thickness and MoS_2 light absorption. Figure 3(a) depicts the evolution of the absorption spectrum with the thickness of the Si_3N_4 layer a_l. Obviously, the absorption peak appears as a red shift with increasing a_l and reaches the maximum when $a_l = 82$ nm. The simulation results coincide well with the TMM calculations. As shown in Fig. 3(b), the absorption of monolayer MoS_2 can reach 95.3% with a full width at half-maximum (FWHM) of ~1.9 nm when $a_l = 82$ nm. To clarify the physical mechanism of the light absorption improvement, we study the electric field intensities in MoS_2 between the Bragg mirrors with different a_l, as plotted in the inset of Fig. 3(b). It is found that the electric field intensity exhibits a maximum when $a_l = 82$ nm, which induces the strongest light-MoS_2 interaction and light absorption in the visible range. Furthermore, we investigate the dependence of MoS_2 light absorption on the thickness a_r and incident angle θ. Figure 3(c) depicts the evolution of the absorption spectrum with a_r when $a_l = 82$ nm. It shows that the wavelength of the absorption peak possesses a red shift with increasing a_r, and the absorption efficiency can reach the highest value of 95.7% when $a_r = 149$ nm. With increasing the incident angle, there is a blue shift for the absorption peak, as shown in Fig. 3(d). The energy of OTSs rises when increasing θ[25]. Thus, we can observe a blue shift of the absorption peak. Meanwhile, the height of the absorption peak almost remains unchanged. The adjustment of incident angle θ contributes to the flexible selection of the operating wavelength and MoS_2 light absorption.

Moreover, we can see that the light absorption of MoS_2 relies on the period number of Bragg mirror P_l, as depicted in Fig. 4(a).

There is a slight blue shift for the MoS_2 absorption peak with increasing P_l. The blue shift of the absorption peak arises from the deviation of OTS wavelengths with varying P_l. The Bloch-wave-expansion method (BWEM) is introduced to obtain the precise OTS wavelengths and its dependence on the period numbers of two Bragg mirrors[36]. The occurrence of OTSs can be characterized by matching the surface impedances at the interface of two Bragg mirrors, namely, ξ_{left} and ξ_{right}. The match condition can be specified by the wavelength-dependent function, $|\xi_{\text{left}} - \xi_{\text{right}}|$. It is found that the OTS wavelength coincides with the dip wavelength, where $|\xi_{\text{left}} - \xi_{\text{right}}|$ is minimum. The OTS wavelengths (red dashed line with dots) calculated with BWEM are plotted in Fig. 4(b). Since the period number of the left Bragg mirror P_l is relatively small, the increase of P_l will cause a non-negligible change for ξ_{left} in the overlapped band gap of two Bragg mirrors, resulting in a blue shift. As shown in Fig. 4(b), the BWEM theoretical results agree well with the TMM calculations. The minor difference (~1 nm) between the OTS wavelength and MoS_2 absorption peak could be attributed to the insertion of the MoS_2 monolayer. The absorption peak gradually increases as P_l changes from 7 to 9, while it decreases when P_l further increases, as shown in Fig. 4(b). To clarify the mechanism, we analyze the MoS_2 light absorption using the TCMT[37]. According to TCMT, the multilayer system can be treated as a lossy cavity with two ports, as depicted in the inset of Fig. 4(c). The cavity mode with the resonant frequency ω_0 radiates to the left and right ports with the decay rates γ_1 and γ_2, respectively. γ_3 is the internal loss rate due to the dissipative loss of MoS_2. $S_{i\pm}$ ($i = 1$ and 2) are the amplitudes of incoming and outgoing waves coupled with the cavity mode, respectively. There is no light inputting from the right port, namely, $S_{2+} = 0$. The coupled equations can be described as

$$\frac{da}{dt} = (-j\omega_0 - \gamma_1 - \gamma_2 - \gamma_3)a + \sqrt{2\gamma_1}S_{1+}, \tag{4}$$

$$S_{1-} = -S_{1+} + \sqrt{2\gamma_1}a, \tag{5}$$

$$S_{2-} = \sqrt{2\gamma_2}a. \tag{6}$$

Here, a is the amplitude of the cavity mode. The reflection and transmission spectra can be achieved by $R(\omega) = |S_{1-}/S_{1+}|^2$ and $T(\omega) = |S_{2-}/S_{1+}|^2$, respectively. Then, the absorption spectrum of MoS_2 can be obtained as

$$A(\omega) = \frac{4\gamma_1\gamma_3}{(\omega - \omega_0)^2 + (\gamma_1 + \gamma_2 + \gamma_3)^2}. \tag{7}$$

The above parameters γ_1, γ_2, and γ_3 can be obtained by fitting the MoS_2 absorption spectra. Figure 4(c) shows the fitting absorption spectrum when $P_l = 9$, which is in good agreement with the theoretical result. The fitting results in Fig. 4(d) illustrate that the decay rate γ_1 and loss rate γ_3 exhibit a distinct drop with increasing P_l. γ_2 almost remains unchanged and is two orders of magnitude smaller than γ_1 and γ_3 (namely, $\gamma_2 \ll \gamma_1$, γ_3). γ_1 is closest to γ_3 when $P_l = 9$, thereby the ratio of γ_1 and γ_3 can approach a maximum. Therefore, the MoS_2 light absorption can reach the highest value of 96.2% when $P_l = 9$.

Finally, we discuss the influence of period number P_r on the MoS_2 light absorption. As shown in Fig. 4(e), the MoS_2 absorption shows an upward trend, and the increase of peak value slows down as P_r increases. The peak value can approach 99.4% with an FWHM of 1.6 nm when $P_r = 26$. The peak wavelength remains unchanged with varying P_r from 20 to 26. Compared to P_l, P_r is sufficiently large. The surface impedance at the interface of the right Bragg mirror ξ_{right} barely changes in the overlapped band gap of Bragg mirrors. Thus, the wavelength with a minimum $|\xi_{\text{left}} - \xi_{\text{right}}|$ (corresponding to the OTS wavelength) remains at 504.9 nm, and the wavelength of the MoS_2 absorption peak is unchanged (506.0 nm). According to the BEWM calculation, the offset of the $|\xi_{\text{left}} - \xi_{\text{right}}|$ dip can be neglected when P_r increases from 18. In other words, the position of the MoS_2 absorption peak will remain unchanged for $P_r \geq 18$. The fitting

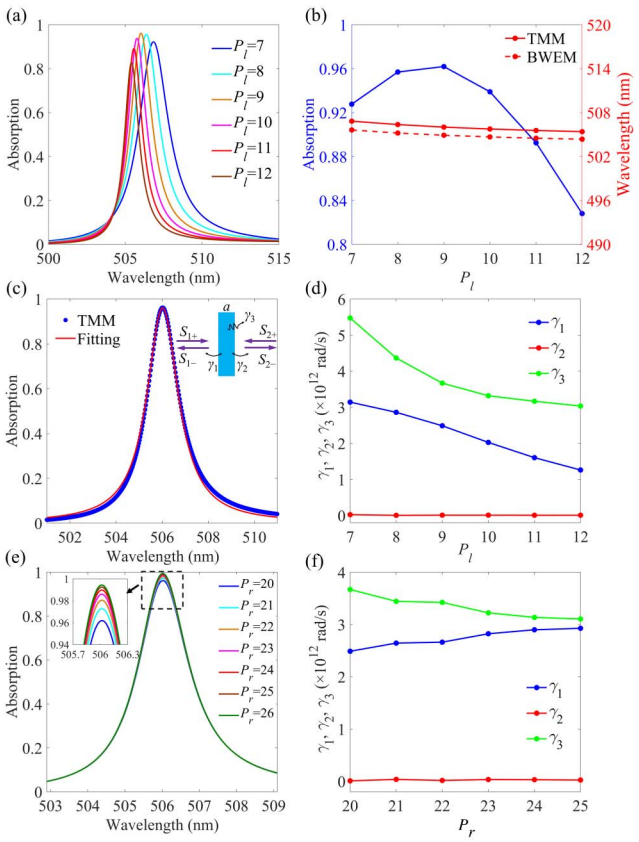

Fig. 4. (a) Light absorption spectra of MoS_2 monolayer in the multilayer structure with different period numbers P_l when $P_r = 20$. (b) Absorption peak values of MoS_2 as a function of P_l, and the wavelengths of MoS_2 absorption peak and OTS as a function of P_l. (c) Absorption spectra of MoS_2 obtained by the TMM calculation (dots) and fitting (line) when $P_l = 9$. The inset shows the TCMT model of OTS in the structure. (d) Fitting parameters γ_1, γ_2, and γ_3 versus P_l. (e) Absorption spectra of MoS_2 in the structure with different P_r when $P_l = 9$. The inset shows the absorption spectra around the peaks. (f) Fitting parameters γ_1, γ_2, and γ_3 versus P_r. Here, $a_l = 82$ nm, $b_l = 44$ nm, $a_r = 149$ nm, $b_r = 130$ nm, and $\theta = 0°$.

parameters in Fig. 4(f) show that γ_2 still remains two orders of magnitude smaller than γ_1 and γ_3. Meanwhile, γ_1 and γ_3 get closer to each other, giving rise to a higher ratio of γ_1 and γ_3. Thereby, the MoS_2 absorption will be infinitely close to one with gradually increasing P_r ($\gamma_1/\gamma_3 \approx 1$).

4. Conclusions

We have investigated the enhanced visible light absorption of the MoS_2 monolayer sandwiched between two different Bragg mirrors with the excitation of the OTS mode. It is distinct from the cavity-supported light absorption enhancement in previous few-layer systems[20,38]. The wavelength and efficiency of MoS_2 light absorption are dependent on the layer thickness of Bragg mirrors, light incident angle, and period numbers of Bragg mirrors. The nearly perfect absorption (99.4%) with an ultra-narrow FWHM of 1.6 nm can be obtained in the structure. The theoretical results are in excellent agreement with the numerical simulations. The BWEM has been applied to analyze the precise alternation of OTS wavelengths with periodic numbers of Bragg mirrors. The TCMT has been used to clarify the mechanism of tailoring MoS_2 light absorption with the period numbers. Our results will pave a new way for the ultra-strong light–matter interaction and favorable applications of atomic-layer materials in highly efficient optoelectronic functionalities, such as photodetection and photoluminescence.

Acknowledgement

This work was supported by the National Key R&D Program of China (No. 2017YFA0303800), the National Natural Science Foundation of China (Nos. 11774290, 11974283, 61705186, and 11634010), and the Natural Science Basic Research Plan in Shaanxi Province of China (No. 2020JM-130).

References

1. A. Geim and K. Novoselov, "The rise of graphene," Nat. Mater. **6**, 183 (2007).
2. Z. Sun and H. Chang, "Graphene and graphene-like two-dimensional materials in photodetection: mechanisms and methodology," ACS Nano **8**, 4133 (2014).
3. Z. Sun, A. Martinez, and F. Wang, "Optical modulators with 2D layered materials," Nat. Photon. **10**, 227 (2016).
4. J. Ponraj, Z. Xu, S. Dhanabalan, H. Mu, Y. Wang, J. Yuan, P. Li, S. Thakur, M. Ashrafi, K. McCoubrey, Y. Zhang, S. Li, H. Zhang, and Q. Bao, "Photonics and optoelectronics of two-dimensional materials beyond graphene," Nanotechnology **27**, 462001 (2016).
5. T. Yang, H. Lin, and B. Jia, "Ultrafast direct laser writing of 2D materials for multifunctional photonics devices," Chin. Opt. Lett. **18**, 023601 (2020).
6. K. Mak and J. Shan, "Photonics and optoelectronics of 2D semiconductor transition metal dichalcogenides," Nat. Photon. **10**, 216 (2016).
7. J. Pei, J. Yang, T. Yildirim, H. Zhang, and Y. Lu, "Many-body complexes in 2D semiconductors," Adv. Mater. **31**, 1706945 (2019).
8. O. Lopez-Sanchez, D. Lembke, M. Kayci, A. Radenovic, and A. Kis, "Ultrasensitive photodetectors based on monolayer MoS_2," Nat. Nanotechnol. **8**, 497 (2013).
9. B. Radisavljevic, A. Radenovic, J. Brivio, V. Giacometti, and A. Kis, "Single-layer MoS_2 transistors," Nat. Nanotechnol. **6**, 147 (2011).
10. Y. Xie, B. Zhang, S. Wang, D. Wang, A. Wang, Z. Wang, H. Yu, H. Zhang, Y. Chen, M. Zhao, B. Huang, L. Mei, and J. Wang, "Ultrabroadband MoS_2 photodetector with spectral response from 445 to 2717 nm," Adv. Mater. **29**, 1605972 (2017).
11. H. Lu, Z. Yue, Y. Li, Y. Zhang, M. Zhang, W. Zeng, X. Gan, D. Mao, F. Xiao, T. Mei, W. Zhao, X. Wang, M. Gu, and J. Zhao, "Magnetic plasmon resonances in nanostructured topological insulators for strongly enhanced light-MoS_2 interactions," Light Sci. Appl. **9**, 191 (2020).
12. H. Zhang, S. Lu, J. Zheng, J. Du, S. Wen, D. Tang, and K. Loh, "Molybdenum disulfide (MoS_2) as a broadband saturable absorber for ultra-fast photonics," Opt. Express **22**, 7249 (2014).
13. Y. Wang, D. Mao, X. Gan, L. Han, C. Ma, T. Xi, Y. Zhang, W. Shang, S. Hua, and J. Zhao, "Harmonic mode locking of bound-state solitons fiber laser based on MoS_2 saturable absorber," Opt. Express **23**, 205 (2015).
14. M. Tsai, S. Su, J. Chang, D. Tsai, C. Chen, C. Wu, L. Li, L. Chen, and J. He, "Monolayer MoS_2 heterojunction solar cells," ACS Nano **8**, 8317 (2014).
15. M. Long, E. Liu, P. Wang, A. Gao, H. Xia, W. Luo, B. Wang, J. Zeng, Y. Fu, K. Xu, W. Zhou, Y. Lv, S. Yao, M. Lu, Y. Chen, Z. Ni, Y. You, X. Zhang, S. Qin, Y. Shi, W. Hu, D. Xing, and F. Miao, "Broadband photovoltaic detectors based on an atomically thin heterostructure," Nano Lett. **16**, 2254 (2016).
16. J. R. Piper and S. Fan, "Broadband absorption enhancement in solar cells with an atomically thin active layer," ACS Photon. **3**, 571 (2016).
17. W. Wang, A. Klots, Y. Yang, W. Li, I. Kravchenko, D. Briggs, K. Bolotin, and J. Valentine, "Enhanced absorption in two-dimensional materials via Fano-resonant photonic crystals," Appl. Phys. Lett. **106**, 181104 (2015).
18. S. Bahauddin, H. Robatjazi, and I. Thomann, "Broadband absorption engineering to enhance light absorption in monolayer MoS_2," ACS Photon. **3**, 853 (2016).
19. X. Luo, X. Zhai, L. Wang, and Q. Lin, "Enhanced dual-band absorption of molybdenum disulfide using a plasmonic perfect absorber," Opt. Express **26**, 11658 (2018).
20. C. Janisch, H. Song, C. Zhou, Z. Lin, A. L. Elías, D. Ji, M. Terrones, Q. Gan, and Z. Liu, "MoS_2 monolayers on nanocavities: enhancement in light-matter interaction," 2D Mater. **3**, 025017 (2016).
21. L. Zhu, F. Liu, H. Lin, J. Hu, Z. Yu, X. Wang, and S. Fan, "Angle-selective perfect absorption with two-dimensional materials," Light Sci. Appl. **5**, e16052 (2016).
22. J. Hu, J. Fu, X. Liu, D. Ren, J. Zhao, and Y. Huang, "Perfect absorption in a monolayer graphene at the near-infrared using a compound waveguide grating by robust critical coupling," Chin. Opt. Lett. **17**, 010501 (2019).
23. D. Jariwala, A. Dayoyan, G. Tagliabue, M. Sherrott, J. Wong, and H. Atwater, "Near-unity absorption in van der Waals semiconductors for ultrathin optoelectronics," Nano Lett. **16**, 5482 (2016).
24. Z. Liu and K. Aydin, "Localized surface plasmons in nanostructured monolayer black phosphorus," Nano Lett. **16**, 3457 (2016).
25. A. Kavokin, I. Shelykh, and G. Malpuech, "Lossless interface modes at the boundary between two periodic dielectric structures," Phys. Rev. B **72**, 233102 (2005).
26. T. Goto, A. Dorofeenko, A. Merzlikin, A. Baryshev, A. Vinogradov, M. Inoue, A. Lisyansky, and A. Granovsky, "Optical Tamm states in one-dimensional magnetophotonic structures," Phys. Rev. Lett. **101**, 113902 (2008).
27. F. Chien, J. Chang, S. Lin, Y. Chou, T. Chen, S. Gwo, T. Chao, and W. Hsieh, "Nanometer-scale conversion of Si_3N_4 to SiO_x," Appl. Phys. Lett. **76**, 360 (2000).
28. J. Xi, J. Kim, and E. Schubert, "Silica nanorod-array films with very low refractive indices," Nano Lett. **5**, 1385 (2005).
29. M. Furchi, A. Urich, A. Pospischil, G. Lilley, K. Unterrainer, H. Detz, P. Klang, A. Andrews, W. Schrenk, G. Strasser, and T. Mueller, "Microcavity-integrated graphene photodetector," Nano Lett. **12**, 2773 (2012).
30. Y. Li, A. Chernikov, X. Zhang, A. Rigosi, H. Hill, A. van der Zande, D. Chenet, E. Shih, J. Hone, and T. Heinz, "Measurement of the optical dielectric function of monolayer transition-metal dichalcogenides: MoS_2, $MoSe_2$, WS_2, and WSe_2," Phys. Rev. B **90**, 205422 (2014).
31. N. Ansari and F. Ghorbani, "Light absorption optimization in two-dimensional transition metal dichalcogenide van der Waals heterostructures," J. Opt. Soc. Am. B **35**, 1179 (2018).
32. M. Kaliteevski, I. Iorsh, S. Brand, R. Abram, J. Chamberlain, A. Kavokin, and I. Shelykh, "Tamm plasmon-polaritons: possible electromagnetic states at the

interface of a metal and a dielectric Bragg mirror," Phys. Rev. B **76**, 165415 (2007).
33. H. Lu, Y. Li, Z. Yue, D. Mao, and J. Zhao, "Graphene-tuned EIT-like effect in photonic multilayers for actively controlled light absorption of topological insulators," Opt. Express **28**, 31893 (2020).
34. H. Lu, X. Gan, B. Jia, D. Mao, and J. Zhao, "Tunable high-efficiency light absorption of monolayer graphene via Tamm plasmon polaritons," Opt. Lett. **41**, 4743 (2016).
35. A. Taflove and S. Hagness, *Computational Electrodynamics: the Finite-difference Time-domain Method* (Artech House, 2005).
36. X. Kang, W. Tan, Z. Wang, and H. Chen, "Optic Tamm states: The Bloch-wave-expansion method," Phys. Rev. A **79**, 043832 (2009).
37. J. Joannopoulos, S. Johnson, J. Winn, and R. Meade, *Photonic Crystals: Molding the Flow of Light*, 2nd ed. (Princeton University, 2008).
38. M. Kats and F. Capasso, "Optical absorbers based on strong interference in ultra-thin films," Laser Photon. Rev. **10**, 735 (2016).